Applied Surface Science 400 (2017) 254–261

Contents lists available at ScienceDirect

Applied Surface Science

journal homepage: www.elsevier.com/locate/apsusc

Full Length Article

Spectroelectrochemical analysis of HOPG surface controlled modification

Esteban A. Franceschini [a,b], Gabriela I. Lacconi [b,*]

[a] Gerencia de Física, Centro Atómico Constituyentes, Comisión Nacional de Energía Atómica, Av. Gral. Paz 1499 (B1650KNA) San Martín, Buenos Aires, Argentina

[b] INFIQC, Dpto. Fisicoquímica, Facultad de Ciencias Químicas, Universidad Nacional de Córdoba, Cdad. Universitaria, 5000 Córdoba, Argentina

ARTICLE INFO

Article history:
Received 3 October 2016
Received in revised form
27 November 2016
Accepted 14 December 2016

Keywords:
Silver electrodeposition
Electrochemical oxidation
SERS
HOPG step edges

ABSTRACT

In situ Raman spectroscopy is used to characterize the changes induced by electrochemical oxidation and silver electrodeposition at the step-edge and terrace sites of highly-oriented pyrolytic graphite (HOPG) surfaces. Ag crystallites are observed to become preferentially deposited onto previously oxidized step edges, thereby leading to an enhancement of the Raman active modes of the HOPG surface. Ex situ Raman spectra recorded after HOPG oxidation exhibit clear differences for both terrace and step-edge areas of the surface. An increase of D and Dí band intensity and two well-defined D-band contributions, D_1 (at 1324 cm^{-1}) and D_2 (at 1344 cm^{-1}), are the main features observed after oxidation. This effect can be correlated with the presence of step-edge sites on the surface, and are found to be strongly dependent on the pH of the solution used in the surface electrochemical oxidation experiments.

1. Introduction

The study of the physicochemical properties of graphite is essential for understanding the properties of new carbon forms, such as graphene, fullerenes, and carbon nanotubes [1]. Recently, a noticeable increase has been observed in the number of technological developments based on aggregates of few graphite layers or graphene sheets, in which edge defects and surface imperfections play an important role [2–4]. The investigation of surface defects is, therefore, of particular relevance to the development of graphite-based nanostructures for device applications.

The surface properties of highly oriented pyrolytic graphite (HOPG) electrodes have been widely studied, mainly by the McCreery and Unwin research groups [5–8]. HOPG is a well-defined model system with an extremely uniform surface, free of metal impurities and pores. Even though electrochemical oxidation in aqueous media leads to modification of surface microstructure and reactivity, HOPG is extensively used as an electrode for the study of several electrochemical reactions [9–11]. It is also well-known that HOPG oxidation occurs most favorably on the edge of steps [7,8,12–14]. There is extensive literature indicating that the electrochemical oxidation of HOPG generates an increase in the number of oxygenated surface groups [15–17]. Pittman and coworkers demonstrated that the rise in surface oxygenated functional groups was mainly due to an increase in carboxyl (COOH) or ester (COOR) groups [18]. The need for understanding the nature of the processes by which different oxygenated functional groups are locally generated on the graphite surface, besides of their potential applications are important incentives to continue the study of these systems.

The surface chemical properties and the quantity and distribution of surface oxygenated groups play a particularly important role in the reactivity of carbon-based materials such as graphene flakes and carbon nanotubes [12,13,19]. In that sense, Fisher and coworkers have conducted experiments of Raman magnifications of carbon surfaces employing metal particles synthesized by microwave plasma chemical vapor deposition [20,21]. The study of carbon stability in the cycling of lithium batteries is a clear example of how the presence of such groups produces changes in the electronic structure of graphite and promotes the activation of heterogeneous electron transfer at the edge plane [8,22]. Additionally, some authors have found that anodic oxidation of HOPG electrodes leads to the breakdown of the graphitic microstructure and increases the step-edge density [23,24]. In recent work, the electrochemical behavior of HOPG in the presence of a redox probe has been monitored at high spatial resolution, revealing modifications on the materials surface, which have been ultimately related to changes of its local electronic and microscopic structure [25].

* Corresponding author.
E-mail addresses: Gabriela.Lacconi1@gmail.com, glacconi@fcq.unc.edu.ar (G.I. Lacconi).

http://dx.doi.org/10.1016/j.apsusc.2016.12.115
0169-4332/

Among the different methods used for surface characterization, Raman spectroscopy has been shown to provide specific information on the microstructure and properties of carbon related materials [26–29]. Raman scattering measurements are non-destructive experiments with enough sensitivity to detect different states of carbon atom hybridization at the graphite surface. The first-order dispersive modes of HOPG surfaces can be detected in the spectral region from 1000 to 1700 cm^{-1}, whereas Raman signals at approximately 1580 cm^{-1} (G band), 1324–1344 cm^{-1} (D band), and 1621 cm^{-1} (Dí band), are the main bands that should be analyzed for a proper characterization of these systems [29]. The G and D/D' bands are related to sp^2 carbon vibrations in the aromatic ring and disorder modes at the edge zone of microcrystalline sheets, respectively. In the second-order spectral region, combination and overtone bands provide complete spectral information. Furthermore, frequency values and intensity ratios of typical (or new) bands at the graphite surface have an important role in the characterization of the material surface structure [1,2,5].

Activation of metal surfaces for surface enhancement of Raman spectroscopy (SERS) has been extensively implemented as a means of enhancing Raman signals at HOPG surfaces [30–34]. Besides, coupling of these spectroscopic methods to an optical microscope has facilitated the recording of recording spectra from sites on the surface, at high sensitivity and resolution. An approach based on simultaneous combining in situ Raman spectroscopy and electrochemical measurements can also be used to gather direct information about the electrode/electrolyte solution interface [35–37].

In this paper, changes in the Raman spectra corresponding to different areas on the HOPG surface, such as those with high density of step edges (**SE**) or terraces (**T**), induced by selective electrochemical oxidation, are investigated by ex situ and in situ experiments. Oxygenated functional groups electrochemically generated at the surface are detected by the spectral differences observed between oxidized step-edge (**SEox**) and oxidized terrace (**Tox**) zones. The anodic oxidation of **SE** areas increases the susceptibility of defect sites towards silver electrochemical nucleation, and the **SE** ability to catalyze electron transfer to Ag^+ ions during the formation of silver SERS-active crystallites. This selective nucleation enables the highly sensitive detection of specific vibrational modes of the **SE** area. The most significant features, which have been found to be strongly dependent on the solution pH and electrode potential, correspond to the presence of two clearly defined contributions for the D band (1324 and 1344 cm^{-1}), and the Dí band (1621 cm^{-1}) close to the G band.

2. Experimental section

All solutions were prepared with Millipore Milli-Q water and analytical grade reagents. The electrolytic solutions employed were 0.1 M $KClO_4$ (Carlo Erba) at different pH (3, 6, and 10), and 0.1 M $KClO_4$ (Carlo Erba) + 1.0 mM $AgClO_4$ (BDH Chemicals Ltd.), for anodic oxidation of HOPG and silver electrodeposition, respectively. $HClO_4$ (Carlo Erba) and KOH (Anhedra) were used to adjust the solution pH. Aqueous solutions were degassed using high purity N_2 (Indura S.A.) before their use in experiments.

HOPG (SPI Supplies, Brand Grade SPI-1) was cleaved with adhesive tape prior to each experiment in order to have a fresh surface. All electrochemical measurements were performed in a single compartment three electrode cell with access for the confocal microscope objective. The HOPG was placed at the bottom of the Teflon cell exposing an area of 0.43 cm^2. A platinum wire ring and a saturated calomel electrode (SCE) or Ag/Ag^+ (1.0 mM) were used as counter electrode and reference or quasi-reference electrode, respectively. The SCE was employed for anodic oxidation of HOPG surface, while the Ag/Ag^+ (1 mM) electrode was utilized for silver electrodeposition experiments. The potential range is indicated in the text and figures along with the reference electrode employed in each case. The difference between the two reference electrodes used is given as $E_{Ag/Ag^+} = -0.30$ V vs. SCE.

For the recording of Raman spectra, laser radiation was focused on two different regions on the HOPG surface: plain terrace (**T**) and high density of step-edge (**SE**) areas. Oxidation of the surface was carried out with a single potential pulse at +1.1 V_{SCE} during 5 s in $KClO_4$ solutions at different pH (3, 6, and 10), thereby generating **Tox** and **SEox** areas. The spectroscopic characterization of the HOPG surface before and after oxidation was performed by conducting ex situ Raman measurements in air and at room temperature. This arrangement was required to set adequate experimental conditions for the in situ study.

Electrochemical measurements were carried out using an Autolab (PGSTAT30 ECOCHEMIE) potentiostat/galvanostat or a CH Instruments Inc. 600E potentiostat/galvanostat for the oxidation before ex situ Raman or during in situ Raman analysis, respectively.

Raman spectra were acquired with a LABRAM-HR, Horiba Jobin-Yvon Raman microscope with a 100× objective lens (NA = 0.9). The 632.8 nm (He-Ne) wavelength was used for laser excitation, with 5 mW power in order to avoid laser induced heating. The illuminated area in all Raman experiments was 1.0 μm^2 with a spectral resolution of 1.5 cm^{-1}. The acquisition time was 10 s, taking the average of 10 spectra.

Ex situ SERS measurements were performed using samples electrochemically oxidized in solutions of different pH. These spectra were represented as normalized signal intensities (by integrated area), using the G band at 1580 cm^{-1} as reference.

In situ SERS spectra of **SE** areas, on which a 50× objective lens (NA = 0.45) was specifically focused, were recorded by applying simultaneously a complex potential-time program with a series of potential steps, in which the electrode surface was firstly oxidized and then silver crystallites were electrodeposited and electrodissolved. Measurements were conducted in aqueous 0.1 M $KClO_4$/1 mM $AgClO_4$ solution at pH 3, using a Teflon cell with an *ad hoc* design for the confocal microscope configuration. The study of electroforming of Ag nanoparticles at pH 6 and 10 could not been carried out, since silver is oxidized at pH values higher to 5.5 with dissolution of particles [38,39]. For this reason, the in situ SERS study with silver particles was only performed at pH 3. In situ spectra were normalized using as reference, the symmetric stretching mode of ClO_4^- ions (932 cm^{-1}), except where absolute values are specified. Raman intensity values presented in this article correspond to the band integral area after baseline corrections and fitting based on Lorentzian functions.

Scanning electron microscopy images were obtained using a Supra 40 (Zeiss Company) FE-SEM Σigma operating at 8 kV.

3. Results and discussion

3.1. Electrochemical oxidation of SE areas

The electrochemical oxidation of the HOPG surface was carried out by applying a potential pulse at 1.1 V_{SCE} during 5 s in 0.1 M $KClO_4$ solution at pH 3.0, 6.0, and 10.0. After anodic modification, cyclic voltammetry (CV) measurements were conducted in the corresponding electrolyte solutions. Fig. 1 shows the CV for HOPG at different pH, with the potential scan ranging between −0.1 and 0.7 V_{SCE}, and starting at 0.4 V_{SCE} and proceeding in the negative direction at 0.02 V s^{-1} scan rate. Noticeable changes in the onset potential for hydrogen evolution are observed for different pH values (not shown), and the formation of oxygen-containing groups on different surface sites at potential more positive than 0.1 V_{SCE}

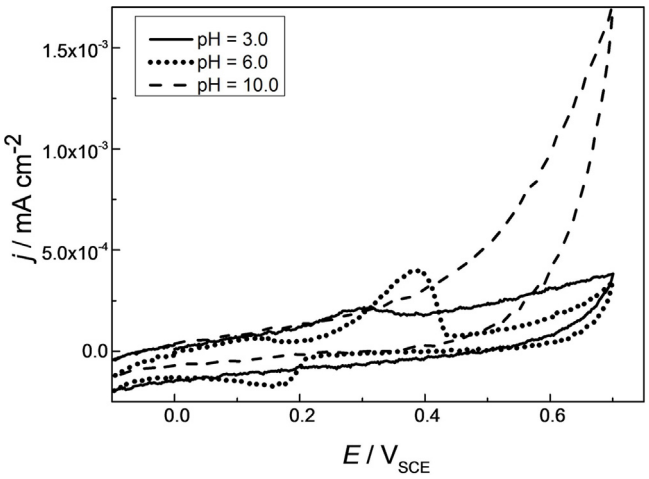

Fig. 1. Cyclic voltammograms of HOPG electrodes in 0.1 M $KClO_4$ solutions at different pH. Electrodes previously oxidized at 1.1 V_{SCE} for 5 s in the corresponding electrolyte solutions. Potential scan rate: 0.02 V s^{-1}.

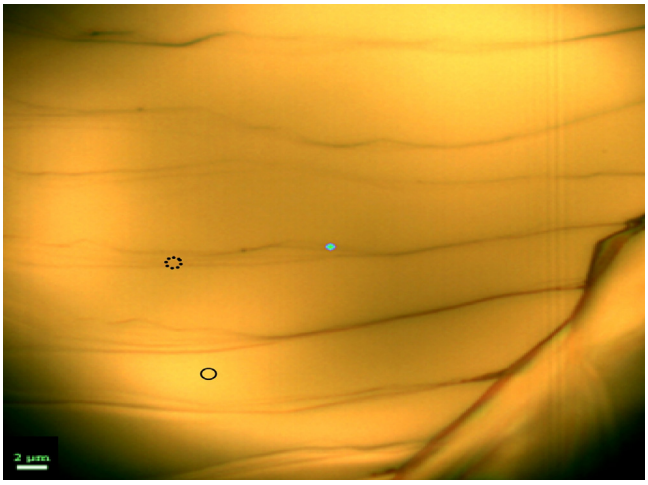

Fig. 2. Optical image of the HOPG surface including areas containing terraces, **T**, and areas with high density of step edges, **SE**, highlighted as filled and dotted circles, respectively.

is clearly distinguished [8,12,23]. In electrolyte solutions of pH 3.0 and 6.0, the current density for the hydrogen evolution reaction is increased with simultaneous detection of oxidation/reduction peaks in the potential region between 0.10 and 0.45 V_{SCE}. At pH 10.0, these current peaks are not clearly visible in the voltammograms. It is well known that anodization of freshly cleaved HOPG surfaces introduces edge site defects and formation of oxygenated functional groups at the electrode surface [29]. It has also been reported in literature that the oxygenated sites on the HOPG surface are more reactive than those present in the freshly cleaved surface [19,22–24]. The absence of oxidation/reduction processes at pH 10 may be explained on the basis that, in highly alkaline solutions, the entire graphitic surface (terraces and edges) can be completely coated with hydroxyl groups, such as in a complete surface passivation with no sites remaining available for further oxidation. This particular effect is the subject of a separate publication.

3.2. Ex situ Raman spectroscopy

Information on the surface structure and chemistry can be obtained by conducting ex situ Raman spectroscopy measurements of the HOPG samples after anodic oxidation. The electrodes initially oxidized at 1.1 V_{SCE} during 5 s in $KClO_4$ solutions were rinsed with water and dried before ex situ Raman spectra were recorded. Fig. 2 shows an optical image of the HOPG surface where two representative areas are indicated by rings. The optical objective was focused on both, **T** and **SE** areas at different points on the surface, in order to record representative Raman spectra. The black rings in the image represent the position of the laser spot (1 μm^2) on **T** (filled ring) and **SE** (dotted ring) selected areas of HOPG surface, for which spectroscopic data were obtained.

In Fig. 3a, ex situ Raman spectra recorded from specific areas both before (**T** and **SE**) and after (**Tox** and **SEox**) anodic oxidation in $KClO_4$ solutions at pH 6.0, are shown. The Raman spectra from **T** and **Tox** areas are practically identical, with characteristic bands from the E_{2g} mode (G band) and the second order signals at 1580, 2642, and 2685 cm^{-1}, respectively. Spectra from terraces show a noticeable increase of the G band intensity. In addition, poor definition of D (at ~1342 cm^{-1}) and Dí (at ~1619 cm^{-1}) bands is noticed in the spectra, which is attributed to the presence of defects within the laser illuminated area (Fig. 3b). These results are consistent with assignments of Raman signals given in the literature [26,29]. Normalized integrated band areas exhibit a variation of less than 0.1%

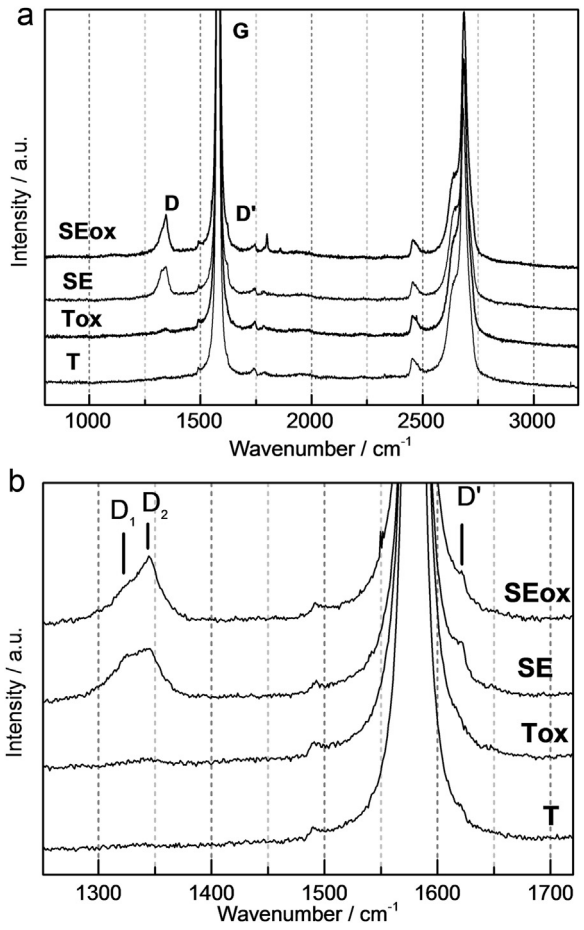

Fig. 3. Comparison of ex-situ Raman spectra, in **a)** 800–3200 cm^{-1} and **b)** 1250–1720 cm^{-1} ranges, for **T** and **SE** areas before and after anodic oxidation at pH 6.0.

when compared across five different points recorded from every specific area of the surface.

Spectra from the **SE** area in Fig. 3a exhibit the same signals as those from the **T** sites (at 1580, 2642, and 2685 cm^{-1}), but with a high contribution from the complex signal originating from the presence of defects (D band). Two components, D_1 and D_2, at 1324

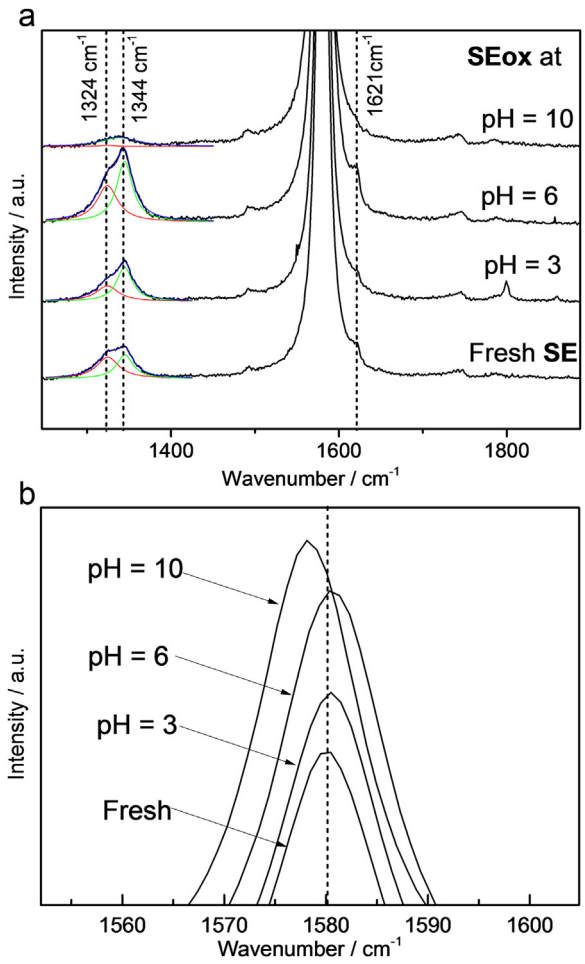

Fig. 4. Ex-situ Raman spectra of HOPG **SEox** obtained after electrochemical oxidation at different pH. For comparison, the spectrum for the **SE** area of a freshly exfoliated HOPG is also shown.

and 1344 cm^{-1}, respectively, are clearly evident before oxidation [26]. Both D_1 and D_2 bands on HOPG surfaces have been observed in previous studies. Compagnini et al. [40] have assigned the D_1 band to a typical edge-plane related process and the D_2 band (disorder-related) to a process dependent on the amount of defects introduced after ion-implantation into HOPG. In addition, evidence of a Dí band (1619 cm^{-1}), which is associated with the D_2 contribution, is clearly visible in the **SE** spectrum [5]. In Fig. 3b, the spectrum from **SEox** shows that the relative intensities of D_2 and D_1 components are modified by anodic oxidation of the surface. Thus, the 2D band intensity from step edge and terrace areas spectra becomes increased (Fig. 3a).

The electrochemical modification of the HOPG surface performed with a potential pulse at 1.1 V_{SCE} leads to soft oxidation of the surface, being favored the formation of carbonyl, ether, and hydroxyl groups at the step edges [5,41]. The most significant features revealed by the comparison of **SE** and **SEox** spectra can be summarized as: (i) modification of the relative intensities between D_1 and D_2 components of the D band, (ii) slight increase in the absolute intensity of the G band, (iii) detection of Dí band at 1621 cm^{-1}, and (iv) increase in the intensity of bands at 2643 cm^{-1} and 2685 cm^{-1}, in the second-order region.

Fig. 4a shows spectra obtained from **SEox** areas (with results from **Tox** areas not being shown) after anodic oxidation in 0.1 M $KClO_4$ solutions at pH 3, 6, and 10. For comparison, the spectrum from a step edge area of a freshly exfoliated surface is also included. In Table 1 the D/G and 2D/G intensity ratios are presented. It can

Table 1
D/G and 2D/G intensity ratios from step edges sites oxidized at different pH. Data corresponds to ex situ spectra of Fig. 4a and are normalized at the G band corresponding to each spectrum.

Oxidation pH	I_D/I_G	I_{2D}/I_G
Fresh exfoliated	9.2	96.8
pH 3	9.7	88.8
pH 6	12.9	84.2
pH 10	2.4	95.4

be observed that after oxidation at pH 3 and 6 the intensity of the D-band increases markedly, whereas that of 2D band certainly decreases. This tendency is reversed when the oxidation process is carried out at pH 10. Moreover, the D_1/D_2 intensity ratio, when the oxidation is performed in electrolyte solutions of pH 3 is higher than that at pH 6. This trend may be explained on the basis of changes to the type or amount of oxygenated functional groups at the edges. However, both contributions, D_1 and D_2, are similarly evident with equivalent intensities to those from a freshly cleaved HOPG surface.

On the other side, oxidation of **SE** areas in alkaline solutions (pH 10) results in very weak D_1 and D_2 signals and a more symmetric G band, which suggests that at pH 10 the amount of defects at the edges has not increased. This process could be alternatively investigated by in situ measurements (see next sections) after silver deposition at the steps. However, the formation of silver oxide complicates the measurement at pH 10. It is also possible that after surface oxidation in highly alkaline solutions, the presence of surface defects may not be easily established by spectroscopic measurements. Another feature in Fig. 4b is the red shift of the G band ($\sim 2\,cm^{-1}$) in the spectra at pH 10, which may indicate an increase of the amount of sp^3 carbon because of the large number of oxidized groups.

These spectral data can be analyzed on the basis of the potentiodynamic behavior showed in Fig. 1, by correlating the D_2 band integral area with the oxidation charge in the voltammograms at each pH (anodic peak between 0.25 and 0.45 V_{SCE}). The intensity of this band is actually observed to increase as the oxidation charge becomes higher. It has been mentioned that samples oxidized at pH 10 exhibit the lowest oxidation charge and that the Dí band is practically absent in the spectra. However, although the electrochemical behavior of previously oxidized HOPG electrodes is dependent on the solution pH (Fig. 1), a direct comparison with the effect observed in the spectra is not possible, because the electrochemical results represent an average across the entire electrode area (including both terrace and step-edge areas), while Raman scattering originates from localized regions delimited by the size of the laser spot ($\sim 1\,\mu m^2$). Thus, step edges are HOPG defects that can be detected by the presence of D band, when they are preferentially oxidized.

The spectral analysis of changes in the structure of graphite is normally carried out by monitoring the relative intensity between D and G bands [26,29]. Even though the information in each spectrum in Fig. 4 comes from different samples and therefore, from distinct **SE** regions on the surface, a significant increase of I_{D2}/I_G and $I_{Dí}/I_G$ ratios is observed as the voltammetric oxidation charge of step edges increases and the pH for oxidation changes from 3 to 6. These Raman scattering results are indicative of a larger amount of surface defects when the oxidation is performed at pH 6. Thus, the intensity of D_2 signal is related to the defects produced by the electrochemical oxidation.

However, when anodic oxidation is carried out in alkaline solutions, the intensity of D_1, D_2, and Dí bands becomes significantly diminished. Besides, the sum of the normalized intensities of D_2 and Dí bands exhibits a similar dependence with the anodic oxidation charge that the simple D_2 band (Fig. 5). Data in Fig. 5 are derived from the spectra in Fig. 4, with integrated intensity val-

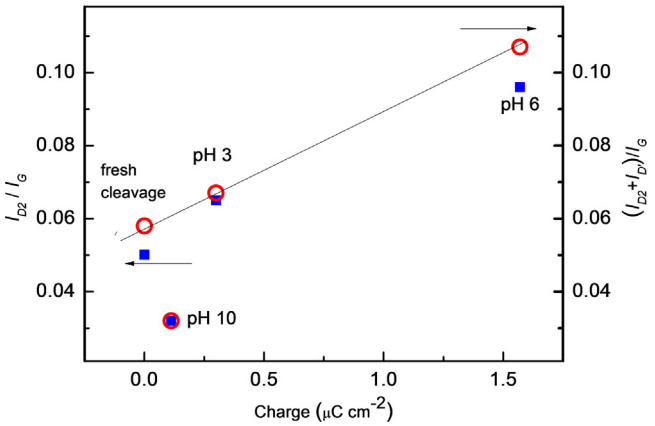

Fig. 5. Plots of I_{D2}/I_G (blue squares) and $(I_{D2}+I_{Di})/I_G$ (red rings) ratios as a function of the electrochemical oxidation charge from voltammograms in Fig. 1. Raman intensity taken from ex-situ configuration spectra of HOPG **SEox**, obtained after electrochemical oxidation at different pH. For comparison, data for the **SE** area of a freshly exfoliated HOPG are also shown. Squares and circles correspond to the I_{D2}/I_G and $(I_{D2}+I_D')/I_G$ axis, respectively. (For interpretation of the references to colour in this figure legend, the reader is referred to the web version of this article.)

ues calculated by a Lorentzian fit to the area of each Raman signal. Some authors have observed these features in the Raman spectra of graphite and have provided different explanations [26,40,42]. Ping et al. have found that the intensity of D_2 band increases when the incident laser polarization plane is parallel to the edge plane of the sample [26]. Moreover, the increase of the D_2 signal (at 1360 cm^{-1} for a 514 nm laser) has also been observed when disorder inside of graphite is introduced by ion irradiation [40]. Katagiri et al. have related these spectral features to the discontinuity of graphite planes detected mainly in the edge plane spectra [42]. Ferrari et al. have also found two components of D peak at the edge of graphite [1].

The two components of D band are clearly evident in the ex situ Raman spectra presented in Figs. 3b and 4a. In agreement with the publications mentioned in the preceding paragraph, the present work indicates that the intensity of the D_2 and D' bands is directly related to the oxygenated functional groups generated by electrochemical oxidation.

3.3. Silver electrodeposition at S*E* areas

After the electrochemical oxidation of the HOPG surface, whereby carbonyl, hydroxyl, ether, and other oxygen-containing functional groups are formed preferentially at the step edges, silver nucleation can be favorably activated at these sites. The presence of these groups on the surface promotes larger affinity of metal adatoms to these sites and therefore, favoring a high density of nuclei at the step edges [6,31,43].

In order to establish the onset potential for silver deposition onto HOPG, the electrochemical behavior was initially analyzed. Fig. 6 shows cyclic voltammograms for a freshly cleaved HOPG electrode in 0.1 M $KClO_4$ + 1 mM $AgClO_4$ solution at pH 3, recorded at a scan rate of 0.001 V s^{-1} and room temperature. In the first cycle two cathodic peaks from Ag^+ ion reduction at −0.2 $V_{Ag/Ag+}$ and −0.6 $V_{Ag/Ag+}$, possibly on different sites on the surface, are observed. In the anodic scan, the silver deposit is electrochemically dissolved at around 0.1 $V_{Ag/Ag+}$. During the second voltammetric cycle, silver electrodeposition is clearly activated and the onset potential is shifted to 0.005 $V_{Ag/Ag+}$. This feature is well-known [44] and has been related to the remaining metal centers on the surface facilitating crystallite growth in the second cycle. Thus, the HOPG surface is irreversibly modified by silver deposition.

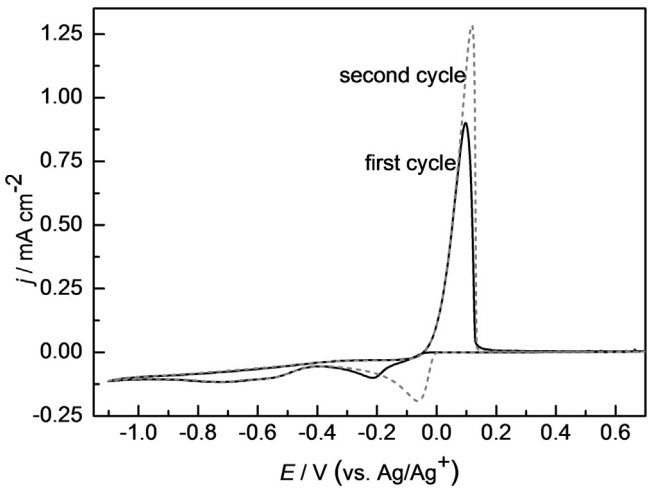

Fig. 6. Cyclic voltammogram (first and second cycles) of HOPG in 0.1 M $KClO_4$ + 1 mM $AgClO_4$ solutions at pH 3.0. Potential scan rate: 0.001 V s^{-1}.

Monitoring of Ag crystallites formation on the oxidized electrode was achieved by Raman spectra recorded during the application of a potential pulses sequence at the electrode in 0.1 M $KClO_4$ + 1 mM $AgClO_4$ solution at pH 3.0 (Fig. 7). Initially, the electrode was held at 1.1 $V_{Ag/Ag+}$ (E_{ox}) for 5 s to oxidize the step edges and, subsequently, a potential of −1.0 $V_{Ag/Ag+}$ (E_{nucl}) for 0.1 s was applied to initiate silver nucleation at these sites. The next pulse was applied at −0.08 $V_{Ag/Ag+}$ (E_{growth}) for 350 s, leading to slow particle growth and, finally, at 0.05 $V_{Ag/Ag+}$ (E_{dissol}) during 500 s, silver particle dissolution was induced.

Fig. 8 shows a SEM image of HOPG electrodes after 350 s of silver electrodeposition at E_{growth} using the program in Fig. 7. Two crystallite families with different size are clearly observed. Many small particles and a limited number of flower-like crystallites are located at the step edges of the HOPG surface. After different times during silver dissolution, the large particles acquire a faceted surface while their size is reduced (not shown).

3.4. In situ SERS spectra from *SEox* areas during silver deposition and dissolution

Electrochemical measurements were performed in $KClO_4$ solution at three different pH (3, 6, and 10), in order to study the effect of pH on the oxygenated groups present at the edges and terraces, whereas spectroelectrochemical experiments in the presence of Ag^+ ions were undertaken at pH 3 to prevent silver particle oxidation.

In situ Raman spectra were recorded during the application of potential pulses (potential-time program given in Fig. 7) at the electrode in two electrolyte solutions at pH 3.0: (i) 0.1 M $KClO_4$ and (ii) 0.1 M $KClO_4$ + 1 mM $AgClO_4$. Enhancement of Raman scattering from the surface occurs due to the presence of silver crystallites constantly growing. Fig. 9 contains the sequence of in situ SERS spectra from **SEox** areas at the HOPG surface. All signals in the 700–1700 cm^{-1} range were normalized with respect to the symmetric stretching band of ClO_4^- ions at 932 cm^{-1} [45]. Successive spectra were recorded in the absence of Ag^+ ions and no significant changes were observed in the Raman spectra when the full potential-time program was applied (Fig. 9). Parallel experiments in solutions containing Ag^+ ions were carried out. Spectra were recorded at different times during silver electrodeposition (labeled A1 through A4) and dissolution (labeled B1 through B4) potential pulses. In the first spectrum, A1, after 50 s of silver nucleation on **SEox** surface, the presence of the Dí band (at 1620 cm^{-1}) related to the step edges, in addition to the G band (at 1580 cm^{-1}), was

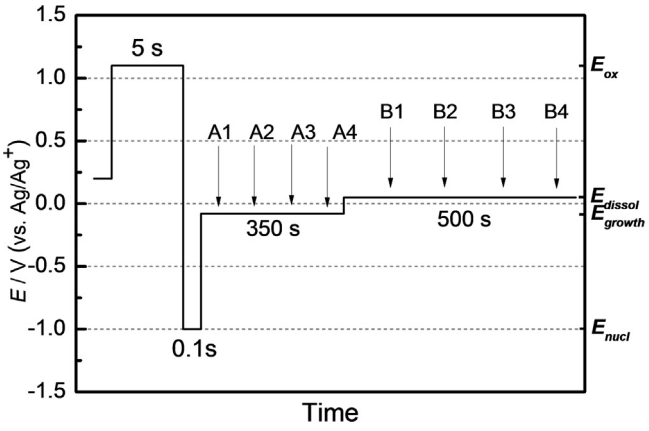

Fig. 7. Potential-time program applied to HOPG electrodes with a sequence of potential pulses: oxidation potential, E_{ox} = 1.1 V (5 s), nucleation potential, E_{nucl} = −1.0 V (0.1 s), growth potential, E_{growth} = −0.08 V (350 s), and dissolution potential, E_{dissol} = 0.05 V (500 s). All potentials are given relative to Ag/Ag^+ (1 mM) quasi-reference electrode. Electrolyte: 0.1 M $KClO_4$ + 1 mM $KClO_4$ at pH 3.0.

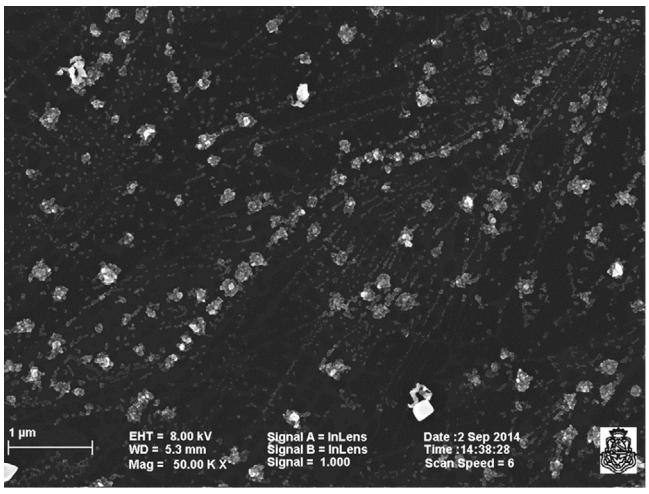

Fig. 8. SEM image of HOPG surface after silver electrodeposition at −0.08 V (350 s) in 0.1 M $KClO_4$ + 1 mM $AgClO_4$ solution at pH 3, by the potential-time program of Fig. 7.

evident. As silver crystallites grow at the **SEox** area, a progressive decrease of G band intensity is noticed (Fig. 9). However, there is an enhancement of Raman scattering generated by the silver particles, either during their growth or dissolution, an effect that can be better appreciated when absolute intensities are compared (see Fig. 10), because the ClO_4^- ions signal is also increased by coadsorption of them. In contrast, SERS spectra recorded during the progressive dissolution of silver particles (spectra B1 to B4) show noticeable changes, such as a decrease in G band intensity and increase of Dí (1622 cm^{-1}) and D_2 (1345 cm^{-1}) bands related to edges. These results are consistent with the SEM image, which shows that deposited particles are mainly localized at defects.

Although in situ spectra in different electrolyte solutions were recorded by focusing on different **SEox** areas at the surface, the series of spectra in each electrolyte solution was obtained at the same point on the surface. This arrangement is of particular importance to the controlled monitoring of the process during the spectroelectrochemical experiment.

We have mentioned that the Raman enhancement can be better appreciated when absolute intensity values are compared. Fig. 10 shows a comparison between the first and last in situ spectra, recorded during application of the full electrochemical program (Fig. 7). All spectra are in the 200–3500 cm^{-1} range for the HOPG **SE** areas in 0.1 M $KClO_4$ (10a) and 0.1 M $KClO_4$ + 1 mM $AgClO_4$ (10b) solutions. After the anodic oxidation in the absence of silver ions, an increase in ClO_4^- signal intensity and decrease in G and 2D bands intensity, with better definition of the Dí signal, are observed. It is possible that, as the electrode potential is modified, the presence of anions in the proximity of the electrode/solution interface could change. Thus, when the potential is maintained at +0.08 V (final spectrum), the interaction of HOPG with ClO_4^- anions may be favored. Moreover, silver nucleation and growth at the step edges leads to an increase in intensity for all signals (Fig. 10b), due to the SERS effect induced by Ag crystallites. Also, the ClO_4^- ions can be coadsorbed on the crystallites, therefore the intensity of the band at

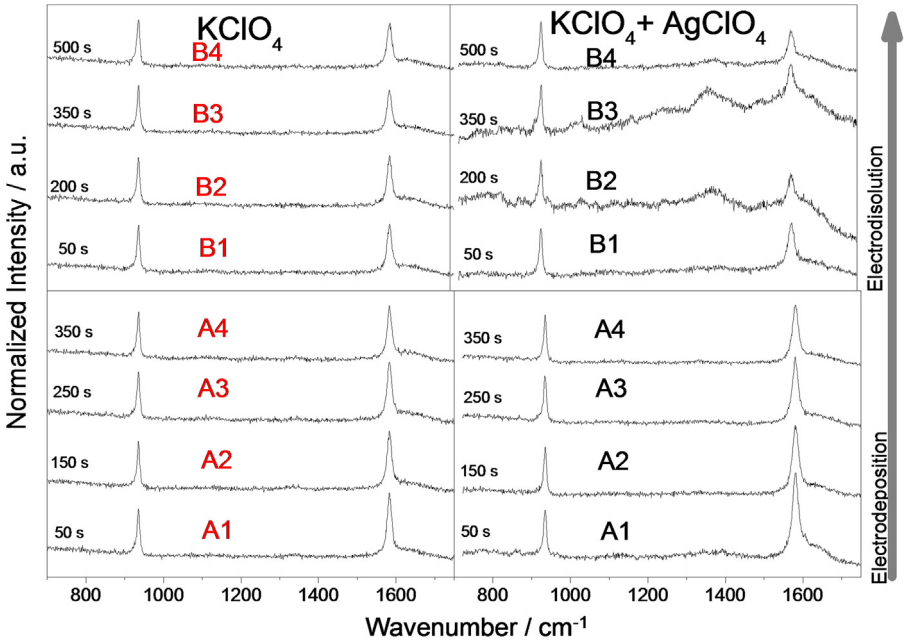

Fig. 9. Sequence of in-situ Raman and SERS spectra of **SEox** area by application of the potential-time program of Fig. 7. Series of spectra **A** and **B** recorded in both 0.1 M $KClO_4$ and 0.1 M $KClO_4$ + 1 mM $AgClO_4$, during silver electrodeposition and dissolution potential steps, respectively.

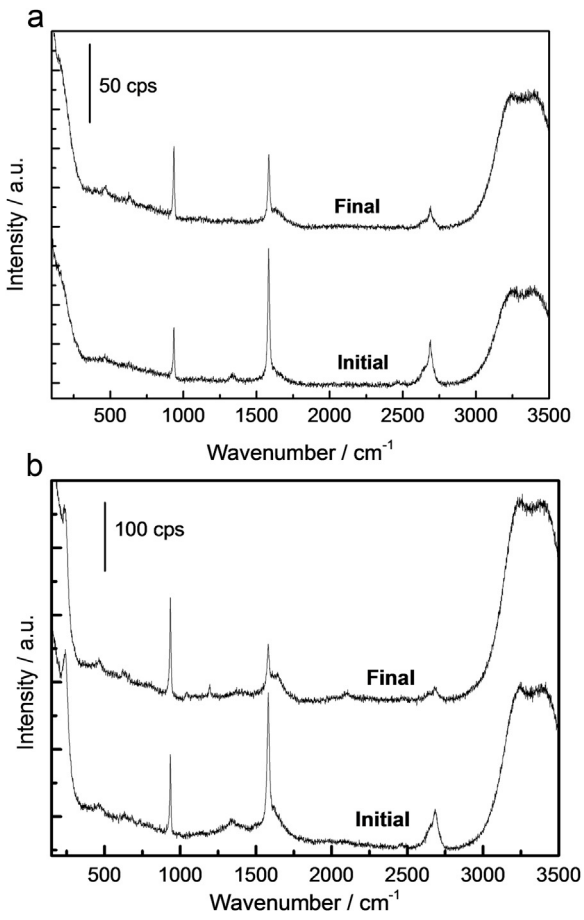

Fig. 10. Raman and SERS in-situ spectra (intensity in absolute values), recorded before and after application of a potential-time program, as in Fig. 7, to the step-edge area of HOPG, in **a)** 0.1 M $KClO_4$ and **b)** 0.1 M $KClO_4$ + 1 mM $AgClO_4$ solutions.

932 cm^{-1} is increased. Another feature observed is the simultaneous increase of D_2 and Dí intensity (with no change in frequency), relative to the spectra in Fig. 10a. This SERS increase in the ClO_4^- signal remains even after silver dissolution and it is almost complete at +0.08 V after 500 s (final spectrum in Fig. 10b). However, under these conditions Raman signals from HOPG become diminished in intensity, indicating that the silver particles remaining on the surface have lower efficiency as SERS active substrates.

4. Conclusions

In the present study, we have reported a spectroelectrochemical investigation of the effect produced by anodic oxidation on the terrace and step-edge zones of HOPG surface. Localized oxidation of the graphite was performed through application of a potential pulse at −1.1 V and typical Raman bands from graphite were subsequently recorded. Ex situ Raman spectroscopy was employed to study the surface structure under different conditions of anodic oxidation, while in situ spectroelectrochemical experiments were conducted to examine the processes of silver deposition and dissolution, at the oxidized sites.

Differences in the Raman spectra of step-edge and terrace areas are related to the surface modification by electrochemical oxidation. Two contributions of D band (at 1324 and 1344 cm^{-1}) and the associated Dí signal (at 1621 cm^{-1}), from the scattering generated by microstructural disorder, were directly correlated with the presence of step-edge sites on the surface, being absent in the spectra of terraces. A brief summary of the relevant features observed is: (i) modification of the relative intensities of D_1 and D_2 components of D band; (ii) slight increase in the absolute intensity of the G band; (iii) presence of a well-defined new band, Dí, at 1621 cm^{-1}, and (iv) decrease in the ratio between integrated bands at 2640 cm^{-1} and 2686 cm^{-1}, in the second-order region.

The intensity increase of D and D' bands observed in the in situ Raman spectra from HOPG **SE** areas is produced by SERS effect generated by silver crystallites during their electrodeposition. Although, the size and form of silver particles are modified throughout the experiment, they are mainly electrodeposited on step edges sites (previously oxidized), at the HOPG surface. We obtain HOPG electrodes with SERS activity regions (areas with high density of **SE** sites), whereby surface defects on the carbon surface, can be detected with high sensitivity.

Conflict of interest

The authors declare no conflict of interest.

Acknowledgements

The authors are grateful to Agencia Nacional de Promoción Científica y Tecnológica, SECyT-UNC, and CONICET, for financial support, to LAMARX laboratory (IFEG-CONICET) for assistance in SEM measurements, and to the Laboratorio de Nanoscopía y Nanofotónica (LANN) at INFIQC-CONICET for access to Raman microscopy facilities. G.L. and E.F. are permanent research fellows of CONICET.

References

[1] A.C. Ferrari, Raman spectroscopy of graphene and graphite: disorder electron-phonon coupling, doping and nonadiabatic effects, Solid State Commun. 143 (2007) 47–57.
[2] M.S.G. Dresselhaus, G. Dresselhaus, K. Sugihara, I.L. Spain, H.A. Goldberg, Graphite Fibers and Filaments, Vol. 5 of Springer Series in Materials Science, Springer-Verlag, Berlin, 1988.
[3] R. Sharma, J.H. Baik, Ch.J. Perera, M.S. Strano, Anomalously large reactivity of single graphene layers and edges toward electron transfer chemistries, Nano Lett. 10 (2010) 398–405.
[4] Y.L. Mikhlina, E.A. Vishnyakova, A.S. Romanchenko, S.V. Saikova, M.N. Likhatski, Y.V. Larichev, F.V. Tuzikov, V.I. Zaikovskii, S.M. Zharkov, Oxidation of Ag nanoparticles in aqueous media: effect of particle size and capping, Appl. Surf. Sci. 297 (2014) 75–83.
[5] R.L. McCreery, Advanced carbon electrode materials for molecular electrochemistry, Chem. Rev. 108 (2008) 2646–2687.
[6] 6Y.-R. Kim, S.C.S. Lai, K. McKelvey, G. Zhang, D. Perry, Th.S. Miller, P.R. Unwin, Nucleation and aggregative growth of palladium nanoparticles on carbon electrodes: experiment and kinetic model, J. Phys. Chem. C 119 (2015) 17389–17397.
[7] G. Zhang, P.M. Kirkman, A.N. Patel, A.S. Cuharuc, K. McKelvey, P.R. Unwin, Molecular functionalization of graphite surfaces: basal plane versus step edge electrochemical activity, J. Am. Chem. Soc. 136 (2014) 11444–11451.
[8] R.J. Bowling, R.T. Packard, R.L. McCreery, Activation of highly ordered pyrolytic graphite for heterogeneous electron transfer: relationship between electrochemical performance and carbon microstructure, J. Am. Chem. Soc. 111 (1989) 1217–1223.
[9] M. Bayati, J.M. Abad, C.A. Bridges, M.J. Rosseinsky, D.J. Schiffrin, Size control and electrocatalytic properties of chemically synthesized platinum nanoparticles grown on functionalized HOPG, J. Electroanal. Chem. 623 (2008) 19–28.
[10] C.R. Bradbury, L. Kuster, D.J. Fermín, Electrochemical reactivity of HOPG electrodes modified by ultrathin films and two-dimensional arrays of metal nanoparticles, J. Electroanal. Chem. 646 (2010) 114–123.
[11] J. Zhang, E. Wang, STM investigation of HOPG superperiodic features caused by electrochemical pretreatment, J. Electroanal. Chem. 399 (1995) 83–89.
[12] R. Penner, in: R.E. White (Ed.), Modern Aspects of Electrochemistry, Vol. 45, Springer, New York, 2009.
[13] G. Dobrik, L. Tapasztó, L.P. Biró, Selective etching of armchair edges in graphite, Carbon 56 (2013) 332–338.
[14] C.I. Vázquez, G.I. Lacconi, Nucleation and growth of silver nanostructures onto HOPG electrodes in the presence of picolinic acid, J. Electroanal. Chem. 691 (2013) 42–50.
[15] P.A. Staley, C.M. Newell, D.P. Pullman, D.K. Smith, The effect of glassy carbon surface oxides in non-aqueous voltammetry: the case of quinones in acetonitrile, Anal. Chem. 86 (2014) 10917–10924.

[16] S.A.C. Carabineiro, M.F.R. Pereira, J.J.M. Órfão, J.L. Figueiredo, Surface chemistry of activated carbons, in: Activated Carbon: Classifications, Properties and Applications, 2011, pp. 125–168.
[17] E. Papirer, E. Guyon, Electrochemical response of the surface oxygenated groups on carbons, Fuel 57 (1978) 123–124.
[18] Z.R. Yue, W. Jiang, L. Wang, S.D. Gardner, C.U. Pittman Jr., Surface characterization of electrochemically oxidized carbon fibers, Carbon 37 (1999) 1785–1796.
[19] A.N. Patel, M.G. Collignon, M.A. O'Connell, W.O.Y. Hung, K. McKelvey, J.V. Macpherson, P.R. Unwin, A new view of electrochemistry at highly oriented pyrolytic graphite, J. Am. Chem. Soc. 134 (2012) 20117–20130.
[20] C.S. Rout, A. Kumar, G. Xiong, J. Irudayaraj, T.S. Fisher, Au nanoparticles on graphitic petal arrays for surface-enhanced Raman spectroscopy, Appl. Phys. Lett. 97 (2010) 133108–133111.
[21] C.S. Rout, A. Kumar, T.S. Fisher, Carbon nanowalls amplify the surface-enhanced Raman scattering from Ag nanoparticles, Nanotechnology 22 (2011) 395704–395711.
[22] K.P. De Jong, J.W. Geus, Carbon nanofibers: catalytic synthesis and applications, Catal. Rev. Sci. Eng. 42 (2000) 481–510.
[23] R. Bowling, R.T. Packard, R.L. McCreery, Mechanism of electrochemical activation of carbon electrodes: role of graphite lattice defects, Langmuir 5 (1989) 683–688.
[24] D.C. Alsmeyer, R.L. McCreery, In situ raman monitoring of electrochemical graphite intercalation and lattice damage in mild aqueous acids, Anal. Chem. 64 (1992) 1528–1533.
[25] A.G. Güell, A.S. Cuharuc, Y.R. Kim, G. Zhang, S.-Y. Tan, N. Ebejer, P.R. Unwin, Redox-dependent spatially resolved electrochemistry at graphene and graphite step edges, ACS Nano 9 (2015) 3558–3571.
[26] P.H. Tan, S. Dimovski, Y. Gogotsi, Raman scattering of non-planar graphite: arched edges polyhedral crystals, whiskers and cones, Phil. Trans. R. Soc. Lond. A 362 (2004) 1–22.
[27] M.S. Dresselhaus, G. Dresselhaus, R. Saito, A. Jorio, Raman spectroscopy of carbon nanotubes, Phys. Rep. 409 (2005) 47–99.
[28] A. Jorio, M.S. Dresselhaus, R. Saito, G. Dresselhaus, Raman Spectroscopy in Graphene Related Systems, Wiley-VCH, Wiley Ed, 2011.
[29] Y. Wang, D.C. Alsmeyer, R.L. McCreery, Raman spectroscopy of carbon materials: structural basis of observed spectra, Chem. Mater. 2 (1990) 557–563.
[30] Y.W. Alsmeyer, R.L. McCreery, Surface-enhanced Raman spectroscopy of carbon electrode surfaces following silver electrodeposition, Anal. Chem. 63 (1991) 1289–1295.
[31] J. Zoval, P.R. Biernacki, R.M. Penner, Implementation of electrochemically synthesized silver nanocrystallites for the preferential SERS enhancement of defect modes on thermally etched graphite surface, Anal. Chem. 68 (1996) 1585–1592.
[32] T. Ito, K. Abe, M. Mohamedi, M. Nishizawa, I. Uchida, In situ SERS spectroscopy of Ag-modified pyrolytic graphite in organic electrolytes, J. Solid State Electrochem. 5 (2001) 328–333.
[33] L. Yan, Y. Yan, L. Xu, R. Ma, F. Jiang, X. Xu, Large range localized surface plasmon resonance of Ag nanoparticles films dependent of surface morphology, Appl. Surf. Sci. 367 (2016) 563–568.
[34] S. Li, X. Yan, Z. Yang, Y. Yang, X. Liu, J. Zou, Preparation and antibacterial property of silver decorated carbon microspheres, Appl. Surf. Sci. 292 (2014) 480–487.
[35] K.G. Schmitt, A.G. Gewirth, In situ surface-Enhanced raman spectroscopy of the electrochemical reduction of carbon dioxide on silver with 3,5-diamino-1,2,4-Triazole, J. Phys. Chem. C 118 (2014) 17567–17576.
[36] C.I. Vázquez, G.F.S. Andrade, M.L.A. Temperini, G.I. Lacconi, Spectroelectrochemical study of picolinic acid adsorption during silver electrodeposition, Electrochim. Acta 156 (2015) 154–162.
[37] C. Mele, B. Bozzini, Silver electrodeposition from water-acetonitrile mixed solvents in the presence of tetrabutylammonium perchlorate, part II, J. Solid State Electrochem. 13 (2009) 1553–1559.
[38] B. Molleman, T. Hiemstra, Surface structure of silver nanoparticles as a model for understanding the oxidative dissolution of silver ions, Langmuir 31 (2015) 13361–13372.
[39] H. Burhanalden Abdulrahman, K. Kołñataj, P. Lenczewski, J. Krajczewski, A. Kudelski, MnO_2-protected silver nanoparticles: new electromagneticnanoresonators for Raman analysis of surfaces in basis environment, App. Surf. Sci. 388 (2016) 704–709.
[40] G. Compagnini, O. Puglisi, G. Foti, Raman spectra of virgin and damaged graphite edge planes, Carbon 35 (1997) 1793–1797.
[41] A. Wieckowski (Ed.), Interfacial Electrochemistry: Theory, Experiment and Applications, Marcel Dekker Inc, New York, 1999.
[42] G. Katagiri, H. Ishida, A. Ishitani, Raman spectra of graphite edge planes, Carbon 26 (1988) 565–571.
[43] E.C. Walter, B.J. Murray, F. Favier, G. Kaltenpoth, M. Grunze, R.M. Penner, Noble and coinage metal nanowires by electrochemical step edge decoration, J. Phys. Chem. B 106 (2002) 11407–11411.
[44] Ma. B. Quiroga Argañaraz, C.I. Vázquez, G.I. Lacconi, Copper electrodeposition onto hydrogenated Si(111) surfaces: influence of thiourea, J. Electroanal. Chem. 639 (2010) 95–101.
[45] J.A. Creighton, M.G. Albrecht, R.E. Hester, J.A.D. Matthew, The dependence of the intensity of Raman bands of Pyridine at a silver electrode on the wavelength of excitation, Chem. Phys. Lett. 15 (1978) 55–58.